

DFT-based Estimation of Damped Oscillation Parameters in Low-Frequency Mechanical Spectroscopy

Krzysztof Duda, Leszek B. Magalas, Mariusz Majewski, and Tomasz P. Zieliński, *Member, IEEE*

Abstract—In this paper, we analyze and compare the properties of different well-known and also new nonparametric discrete Fourier transform (DFT)-based methods for resonant frequency and logarithmic decrement estimation in application to mechanical spectroscopy. We derive a new DFT interpolation algorithm for a signal analyzed with Rife–Vincent class-I windows and also propose new formulas that extend Bertocco and Yoshida methods. We study errors of the resonant frequency and logarithmic decrement estimation in realistic conditions that include measurement noise and a zero-point drift. We also investigate the systematic errors of the estimation methods of interest. A nonlinear least squares time-domain parametric signal fitting is used to determine the boundaries of statistical efficiency in all tests.

Index Terms—Damping estimation, discrete Fourier transform (DFT), frequency estimation, interpolated DFT, logarithmic decrement, mechanical spectroscopy, signal processing.

I. INTRODUCTION

A 1-D second-order differential equation is ubiquitous, well known, and appealing, with a simple interpretation of numerous physical objects, e.g., in materials science, acoustics, and electrical engineering. In this paper, we focus on a physical object investigated by mechanical spectroscopy and estimate the parameters of exponentially damped harmonic oscillations in the presence of noise and a time-dependent zero-point drift (ZPD).

Mechanical spectroscopy is the study of time-dependent responses of stress or strain to various external time-dependent mechanical perturbations (e.g., impulse, quasi-static, or harmonic) through the measurement of any of several different moduli and compliance [1]–[4]. Conventional methods of me-

chanical spectroscopy include low-frequency mechanical spectrometers, vibrating reeds, ultrasonic attenuation, various stress and strain relaxation measurement, etc. The analysis of a free decaying harmonic mechanical response signal obtained from a spectrometer's strain detector requires precise monitoring of the response in the time domain and further numerical treatment of the experimental data. It can be readily shown that a free decay of natural oscillations of an anelastic solid is exponential [1]. A detailed analysis of exponentially damped harmonic oscillations is crucial in mechanical spectroscopy and other spectroscopic techniques such as dielectric spectroscopy, a multiplicity of nuclear magnetic resonance techniques, electric relaxations, etc. All of these techniques measure macroscopic responses due to microscopic motion of atomic, ionic, molecular, and other relaxing entities in the materials under study. These techniques generate experimental data that provide information complementary and supplementary to those from mechanical spectroscopy [2]–[4]. It might be anticipated that each spectroscopic technique faces different experimental difficulties and requires different numerical tools for data analysis. In this paper, we confine ourselves to estimate the parameters of exponentially damped harmonic signals embedded in noise in the presence of a ZPD (trend) [5], [6]. In this paper, we solve this fundamental signal processing problem for the case of a low-frequency mechanical spectrometer (an inverted torsion pendulum, viz., Kê's pendulum) [1], [3].

The problem of estimating in mechanical spectroscopy the resonant frequency f_0 and the logarithmic decrement δ from noise-free decaying oscillations biased by constant offsets and/or time-dependent ZPDs can be (and partially has been already) tackled by several different methods:

- 1) classical and Hilbert transform methods [5]–[10];
- 2) a fitting of discrete data to a model using a nonlinear optimization in the time domain designed by Magalas [8];
- 3) fast discrete-Fourier-transform (DFT)-based methods designed by Yoshida *et al.* [11], Bertocco *et al.* [12], and Agrež [13] that are detailed in the next section and special implementation of the Bertocco method [14];
- 4) a hybrid approach in which an initial estimate is found by a classical algorithm [5], [7]–[9] or a DFT-based estimation method and then is used as a starting point for a nonlinear least squares (NLS) signal fitting to a model.

Other signal processing methods based on direct/modified Prony modeling and linear prediction autoregressive methods

Manuscript received August 24, 2010; revised October 26, 2010; accepted October 28, 2010. Date of publication September 19, 2011; date of current version November 9, 2011. This work was supported in part by the Ministry of Science and Higher Education of Poland under Grant N N507 249040, Grant AGH-11.11.110.013, Grant AGH-11.11.120.543, and Grant AGH-11.11.120.774. The Associate Editor coordinating the review process for this paper was Dr. Wendy Van Moer.

K. Duda is with the Department of Measurement and Instrumentation, AGH University of Science and Technology, 30-059 Kraków, Poland (e-mail: kduda@agh.edu.pl).

L. B. Magalas and M. Majewski are with the Faculty of Metals Engineering and Industrial Computer Science, AGH University of Science and Technology, 30-059 Kraków, Poland (e-mail: magalas@agh.edu.pl; mariuszm@agh.edu.pl).

T. P. Zieliński is with the Department of Telecommunications, AGH University of Science and Technology, 30-059 Kraków, Poland (e-mail: tzielin@agh.edu.pl).

Color versions of one or more of the figures in this paper are available online at <http://ieeexplore.ieee.org>.

Digital Object Identifier 10.1109/TIM.2011.2113124

(originated from the pioneer work of R. Kumaresan and D. Tufts in 1982), combined with low-rank Hankel matrix approximations, singular value decomposition, eigenvalue/subspace analysis, higher order statistics, and many others approaches, have not found application in mechanical spectroscopy mainly due to noise sensitivity and very low accuracy. Therefore, they are not presented and discussed in this paper.

The signal-to-noise (S/N) ratio of strain response signals recorded by modern mechanical spectrometers is 38 dB [5], [8], [9]. It should be emphasized that, in mechanical spectroscopy, very high and repeatable (constant) computation accuracy is required to minimize dispersion (scatter) of experimental points (e.g., δ and f_0). The Yoshida DFT-based logarithmic decrement estimation method [11] and the NLS time-domain signal fitting to a model implemented as an optimization-in-multiple-intervals (OMI) method [8] can be advocated as gold standards in this field. A comparison between classical methods and the OMI algorithm is reviewed in [5] and [7]–[9], whereas advantages of the OMI method are pointed out in [5], [8], and [9].

The goal of this paper is to compare the Yoshida method [11], the most popular DFT-based approach in mechanical spectroscopy [2], [3], with other existing DFT-based algorithms, namely, with the approaches of Bertocco *et al.* [12] and Agrež [13]. We note here that Bertocco did not compare his method to Yoshida's method, although his method was proposed 13 years later, and as demonstrated unequivocally in this paper, the Yoshida method (designed originally for an inverted torsion pendulum) outperforms Bertocco's method. We also propose two new DFT-based methods and point out their advantages and disadvantages. The first method is based on a DFT analysis with Rife–Vincent class-I (RVCI) windows, and its derivation is similar to interpolated DFT methods for undamped sinusoids [15]–[21]. The second approach is based on different order differences of consecutive DFT bins, and it can be treated as an extension of the Yoshida [11] and Bertocco [12] methods. All the results, obtained for simulated data (embedded in 38-dB white noise) are compared with the NLS method as reference.

II. ESTIMATION METHODS

A. Problem Statement

A strain response signal in low-frequency resonant mechanical spectroscopy is described as follows:

$$x(t) = Ae^{-\delta f_0 t} \cos(2\pi f_0 t + \varphi) + \varepsilon_w(t) + \varepsilon_{ZPD}(t) \quad (1)$$

where t is the continuous time in seconds, $A > 0$ is the maximal strain amplitude, f_0 is the resonant frequency in hertz, $-\pi < \varphi \leq \pi$ is the phase in radians, δ is the logarithmic decrement, $\varepsilon_w(t)$ stands for measurement noise, and $\varepsilon_{ZPD}(t)$ denotes the ZPD [5], [6]. The ZPD represents a highly undesirable and dreaded part of the data. The objective of mechanical loss measurement, carried out in mechanical spectrometers, is to estimate the value of the logarithmic decrement δ and the resonant frequency f_0 .

The range of possible values of δ is from 5×10^{-6} to around 2, and the range for the resonant frequency f_0 is from 0.1 to about 10 Hz. The estimation of δ and f_0 is based on

digital representation of (1). Finally, the value of sampling frequency is $f_s = 1$ kHz, and the acquisition time of free decaying oscillations is 30 s in the experimental setup.

The digital representation of (1) has the following form:

$$x[n] = Ae^{-\beta n} \cos(\omega_0 n + \varphi) + \varepsilon_w[n] + \varepsilon_{ZPD}[n] \quad (2)$$

where $x[n]$ stands for the recorded experimental data, $n = 0, 1, 2, \dots, N-1$, $\omega_0 = 2\pi(f_0/f_s)$, and damping $\beta = \delta f_0/f_s$. The angular frequency ω_0 approximately ranges from 0.001 to 0.06 rad, and the number of samples is $N = 30\,000$.

B. Direct Time-Domain Least Squares Optimization

Generally, the problem of estimating β and ω_0 in (2) and, thus δ and f_0 in (1), may be tackled by parametric and non-parametric methods. A straightforward parametric solution is an NLS optimization of a cost function in the time domain defined as

$$C(A, \beta, \omega_0, \varphi, \varepsilon_{dc}) = \sum_{n=0}^{N-1} [x[n] - Ae^{-\beta n} \cos(\omega_0 n + \varphi) - \varepsilon_{dc}]^2 \quad (3)$$

where ε_{dc} stands for an offset. In the case of zero-mean Gaussian noise, the minimization of (3) is a statistically efficient estimator.

In the Magalas method [8], implementation of the time-domain NLS optimization was proposed for high-damping materials that is robust against starting point selection. An NLS Levenberg–Marquardt local optimization procedure is done in the OMI; i.e., first, signal parameters are found using an initial part of the signal, and then, obtained values are used as a starting point in optimization on a larger signal interval (having more samples but starting from the beginning) and so on until the entire data spans are used in the optimization procedure.

In this paper, the NLS method is used to evaluate statistical efficiency of DFT-based algorithms. The time-domain NLS algorithm has clear drawbacks such as difficulty with taking into account arbitrary measurement disturbance in a signal model, high computational cost, and sensitivity to starting point selection in different mechanical spectrometers (mode of vibrations, resonant frequency, shape of a sample, etc.).

C. DFT-Based Methods

The main advantage of nonparametric DFT-based signal parameter estimation is computational efficiency as only one fast Fourier transform of the analyzed signal is required with literally a few extra addition and multiplication procedures. However, it seems pertinent here to remark on the disadvantage of the DFT-based analysis: it is biased by systematic errors caused by spectral leakage and a picket fence effect (detailed discussion on these topics can be found in [22] and [23]). The impact of spectral leakage is substantially reduced using appropriate time windows, whereas picket fence errors are reduced by DFT interpolation algorithms.

The analyzed signal $x[n]$ is assumed to have nonzero values only for indices $n = 0, 1, 2, \dots, N - 1$ and to be zero elsewhere; thus, it can be interpreted as signal $x[n]$ multiplied by the finite-length time window $w[n]$ [22] in the following:

$$v[n] = w[n]x[n] = w[n]Ae^{-\beta n} \cos(\omega_0 n + \varphi). \quad (4)$$

The DFT of signal (4) is defined as

$$V[k] = \sum_{n=0}^{N-1} v[n]e^{-j\omega_k n} \quad (5)$$

where $\omega_k = (2\pi/N)k$, and $k = 0, 1, 2, \dots, N - 1$. If the analyzed signal is observed for a noninteger number of periods, then its angular frequency ω_0 lies either between the DFT bins ω_k and ω_{k+1} or ω_k and ω_{k-1} , where the DFT bin for ω_k has the highest magnitude. The objective of the DFT interpolation algorithm is to determine the frequency correction d , and then, the angular frequency ω_0 of the signal is given by

$$\omega_0 = (k \pm d) \frac{2\pi}{N} \quad 0 < d \leq 0.5. \quad (6)$$

The DFT interpolation problem has several solutions for pure [15]–[21] and damped sinusoidal signals [11]–[14]. The latter is briefly summarized below.

1) *Yoshida Algorithm*: The DFT of sequence (4) with a rectangular window is computed, and the following ratio R is evaluated as

$$R = \frac{V[k-2] - 2V[k-1] + V[k]}{V[k-1] - 2V[k] + V[k+1]}. \quad (7)$$

In (7), four DFT bins with the highest magnitude are used. Damping β and frequency ω_0 are given by

$$\beta = \frac{2\pi}{N} \text{Im} \{-3/(R-1)\}$$

and

$$\omega_0 = \frac{2\pi}{N} \text{Re} \{k - 3/(R-1)\} \quad (8)$$

where k is the index of the DFT bin with the highest magnitude.

2) *Bertocco Algorithm*: The following ratio is used:

$$R = \frac{V[k \pm 1]}{V[k]} \quad (9)$$

where $V[k]$ has the highest magnitude; $V[k+1]$ is in the numerator if $|V[k+1]| \geq |V[k-1]|$, and $V[k-1]$ if otherwise. The frequency correction d and damping β are given by

$$d = \frac{N}{2\pi} \arg\{z\}, \quad \beta = \ln |z| \quad (10)$$

where

$$z = \frac{1-R}{1R \exp(\pm(-j2\pi/N))} \quad (11)$$

and the sign in the denominator is the same as in (9).

3) *Bertocco–Yoshida Algorithm*: In the Yoshida method [11], ratio R is defined using the second-order differences of the DFT bins. Looking from the same perspective, in the Bertocco algorithm [12], the zero-order differences are used. Thus, there is an algorithmic gap since the first-order differences are missing. Therefore, we derive a new estimation algorithm that covers this gap and makes use of the ratio as follows:

$$R = \frac{V[k-1] - V[k]}{V[k] - V[k+1]}. \quad (12)$$

Then

$$\lambda = e^{j\omega_k} \frac{r-R}{re^{-j2\pi/N} - Re^{j2\pi/N}}$$

$$r = \frac{-e^{-j\omega_k} + e^{-j\omega_{k-1}}}{-e^{-j\omega_{k+1}} + e^{-j\omega_k}} \quad (13)$$

and damping and frequency are computed as

$$\beta = -\text{Re} \{\ln(\lambda)\} \quad \text{and} \quad \omega_0 = \text{Im} \{\ln(\lambda)\}. \quad (14)$$

Derivation of the aforementioned algorithm as well as an interpolation formula for third-order differences is given in Appendix A. We refer to this method as Bertocco–Yoshida, and, in all figures, denote it by BY- M , where M is the method's order. The special cases of the BY- M method are BY-0, which is the Bertocco method, and BY-2, which is the Yoshida method.

4) *Agrež Algorithm*: The frequency correction d is estimated by a three-point interpolation DFT algorithm with a Hann window designed for undamped sinusoids [19] as follows:

$$d = 2 \frac{|V[k+1]| - |V[k-1]|}{2|V[k]| + |V[k-1]| + |V[k+1]|} \quad (15)$$

where $V[k]$ is the DFT bin with the highest magnitude. The damping β is estimated from (18) with $M = 0$ or $M = 1$.

5) *Rife–Vincent Algorithm*: In this paper, we propose a new DFT interpolation formula for the signal analyzed with RVC windows of an arbitrary order. The methods aforementioned use either a rectangular (RVC order 0) or a Hann (RVC order 1) window. The RVC windows are cosine windows defined as

$$w_M[n] = \begin{cases} \sum_{m=0}^M (-1)^m A_w[m] \cos\left(\frac{2\pi}{N} mn\right) \\ 0, \quad \text{if otherwise} \end{cases} \quad (16)$$

where $n = 0, 1, 2, \dots, N - 1$, and coefficients $A_w[m]$ are given, e.g., in [17] and [21]. For $M = 0$ and $A_w[m] = 1$, we get the rectangular window $w_0[n] = 1$ in (16). For $M = 1$ and $A_w[m] = [1; 1]$ we get the Hann window $w_1[n] = 1 - \cos((2\pi/N)n)$. The RVC windows are also defined in [23] as $\cos^\alpha(X)$, with $\alpha = 0, 2, 4, 6, \dots$ windows. They have the fastest decay of sidelobes. For higher values of M , the estimation methods are more accurate in noise-free conditions; however, in a noisy environment, they have significantly higher variance.

The frequency correction for the damped sinusoidal signal analyzed with the RVC order M window equals as

TABLE I
SUMMARY OF THE DFT INTERPOLATION FORMULAS

Method	Ratio of DFT bins $V[k]$	Resonant frequency $f_0 = f_s (k \pm d)/N$ or $f_0 = f_s \omega_0/(2\pi)$	Logarithmic decrement $\delta = \beta f_s / f_0$
Bertocco (BY-0) [12]	rectangular window $R = \frac{V[k \pm 1]}{V[k]}, z = \frac{1-R}{1 - R \exp(\pm(-j2\pi/N))}$	$d = \frac{N}{2\pi} \arg\{z\}$	$\beta = \ln z $
Proposed (BY-1)	rectangular window $R = \frac{V[k-1] - V[k]}{V[k] - V[k+1]}$ $\lambda = e^{j\omega_0} \frac{r-R}{re^{-j2\pi/N} - Re^{j2\pi/N}}$ r given by (13)	$\omega_0 = \text{Im}\{\ln(\lambda)\}$	$\beta = -\text{Re}\{\ln(\lambda)\}$
Yoshida (BY-2) [11]	rectangular window $R = \frac{V[k-2] - 2V[k-1] + V[k]}{V[k-1] - 2V[k] + V[k+1]}$	$d = \text{Re}\{3/(R-1)\}$	$\beta = \frac{2\pi}{N} \text{Im}\{-3/(R-1)\}$
Proposed (BY-3)	rectangular window $R = \frac{V[k-2] - 3V[k-1] + 3V[k] - V[k+1]}{V[k-1] - 3V[k] + 3V[k+1] - V[k+2]}$ $\lambda = e^{j\omega_0} \frac{r-R}{re^{-j2(2\pi/N)} - Re^{j2(2\pi/N)}}$ r given by (A7)	$\omega_0 = \text{Im}\{\ln(\lambda)\}$	$\beta = -\text{Re}\{\ln(\lambda)\}$
Agrež [13]	Hann window (RVCI, $M=1$) $R = 2 \frac{ V[k+1] - V[k-1] }{2 V[k] + V[k-1] + V[k+1] }$	$d = R$ (three-point interpolation for undamped sinusoids)	Same as proposed RVCI- M for $M=0$ or $M=1$
Proposed (RVCI- M)	RVCI window, arbitrary order M $R_1 = \frac{ V[k+1] ^2}{ V[k] ^2}, R_2 = \frac{ V[k-1] ^2}{ V[k] ^2}$	$d = -\frac{2M+1}{\frac{R_1 - R_2}{2(M+1)R_1R_2 - R_1 - R_2 - 2M}}$	$\beta = \frac{2\pi}{N} \sqrt{\frac{(d+M)^2 - R_1(d-M-1)^2}{R_1 - 1}}$, $d \neq 0.5$

follows:

$$d = -\frac{2M+1}{2} \frac{R_1 - R_2}{2(M+1)R_1R_2 - R_1 - R_2 - 2M} \quad (17)$$

and damping is given by

$$\beta = \frac{2\pi}{N} \sqrt{\frac{(d+M)^2 - R_1(d-M-1)^2}{R_1 - 1}} \quad d \neq 0.5 \quad (18)$$

with

$$R_2 = \frac{|V[k-1]|^2}{|V[k]|^2}$$

and

$$R_2 = \frac{|V[k-1]|^2}{|V[k]|^2}. \quad (19)$$

The derivation of (17) and (18) is outlined in Appendix B. It is worth mentioning that (18) is consistent with the formulas presented in [13] for the rectangular and Hann windows, i.e., for $M=0$ and $M=1$. The significant difference between our algorithm and the one presented in [13] is that we derived a new formula for the frequency correction d in (17), which is used in (18), whereas in [13], the three-point DFT interpolation algorithm designed for an undamped sinusoids is exploited in (18).

It is observed in (18) that, for $d=0.5$, this equation reduces to $\beta(d=0.5) = 2\pi(0.5+M)/N$, which is incorrect, as damping does not depend on DFT bins anymore. This property of (18) is not discussed in [13]. A practical remedy in such a case is to append a zero-value sample at the end of the analyzed signal; this causes change in the DFT frequency step and also in the value of frequency correction d . In our implementation, we append 0 to the signal if $|0.5-d| < 10^{-4}$. In the following, we denote the proposed algorithms (17)–(19) by RVCI- M , where M is the method's order, i.e., the order of the RVCI window.

The summary of the DFT-based interpolation formulas is given in Table I. In the case of RVCI- M , we have two-step estimation: Frequency correction and damping that depends on the frequency correction. This leads to higher variance of the damping estimation as compared with the BY- M methods where both parameters are obtained in a single step.

III. SIMULATIONS

In this section, we analyze the propagation of the measurement errors through the estimation algorithms and compare it with the optimal NLS estimator (3). We used NLS implemented by the MATLAB *fit* function from the Curve Fitting Toolbox. Starting values for the NLS optimization were taken from the proposed interpolation formulas (17) and (18) with RVCI- $M=1$. During simulations, the mean time of the NLS optimization was approximately 140 times longer than the mean time of the DFT-based estimation.

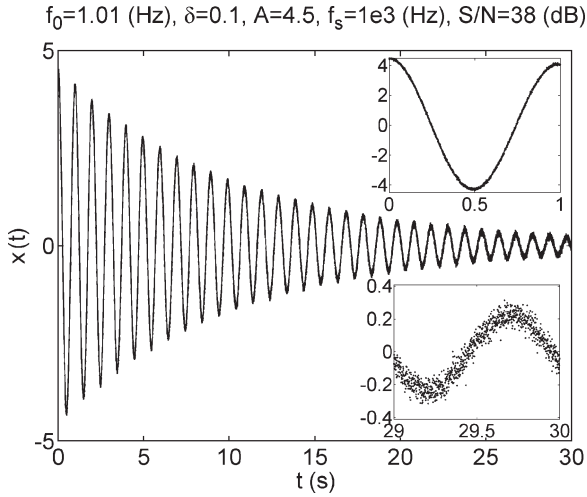


Fig. 1. Exemplary free decaying test signal disturbed by additive noise.

Disturbance $\varepsilon_w(t)$ is real valued zero-mean Gaussian noise with variance σ^2 . The S/N ratio for the exponentially damped sinusoidal signal in decibels is defined as [14], [24]

$$S/N = 10 \log_{10}(\eta) \text{ dB} \quad \eta = A^2/(2\sigma^2). \quad (20)$$

Since the S/N ratio of a low-frequency modern mechanical spectrometer (e.g., a torsion pendulum) is approximately on the level of 38 dB [5], [7]–[9] the test signals were embedded in such noise. In each case, 100 test signals were generated with a random phase with uniform distribution from $-\pi$ to π rad and disturbed by additive noise.

The analyzed errors are computed as $\text{err}_\delta = \delta_E - \delta$ and $\text{err}_{f_0} = f_{0E} - f_0$, where δ and f_0 and δ_E and f_{0E} are true and estimated values, respectively.

Note, that parameters δ and f_0 of the continuous model (1) are estimated from sequence (2); thus, first, damping β_E is estimated, and next, the logarithmic decrement $\delta_E = \beta_E f_s / f_{0E}$ means that the error of the f_0 estimation propagates into the δ estimation.

Fig. 1 depicts an exemplary test signal disturbed by additive 38-dB Gaussian noise. In simulations, the entire range of experimentally measured values of δ from 0.0001 to 0.01 is considered. For the observation time, 30-s test signals with δ smaller than 0.001 looks like undamped sinusoids, i.e., the damping is very small for a visible graphical illustration.

A. Influence of the Logarithmic Decrement

In this section, we analyze estimation errors for test signals with $f_0 = 1.01$ Hz for different values of δ .

The test signals are noncoherently sampled, and the frequency correction is $d = 0.3$.

Figs. 2 and 3 and Figs. 4 and 5 show the maximum error and the standard deviation (STD) of f_0 and δ estimation as a function of δ , respectively. In Fig. 3, the STD for the Bertocco method is on the level above 8×10^{-5} , and for this reason, it is not visible. An increase in $\text{std}(f_{0E})$ observed in Fig. 3 for higher values of δ is caused by the high damping level β .

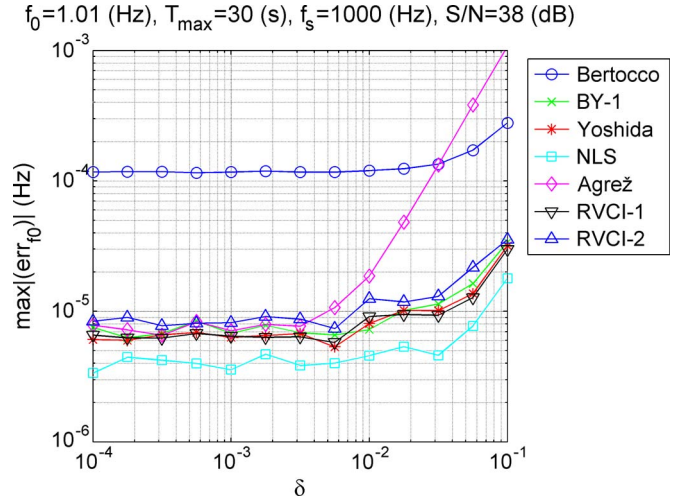


Fig. 2. Maximum error of the resonant frequency estimation.

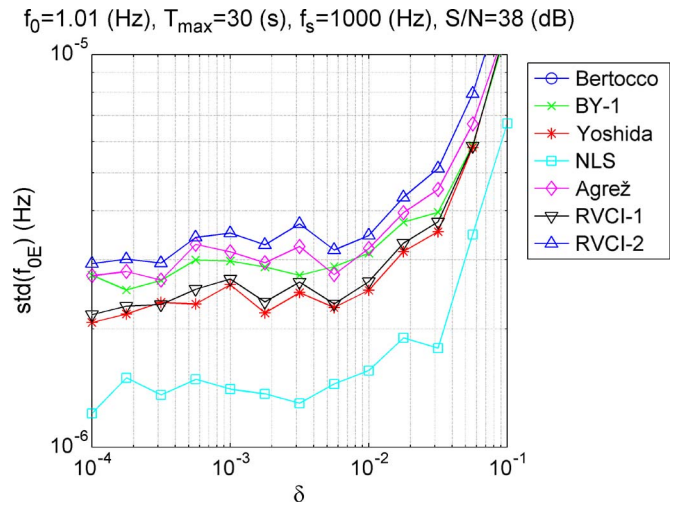


Fig. 3. STD of the resonant frequency estimation. The Bertocco method is out of scale on the level above 8×10^{-5} .

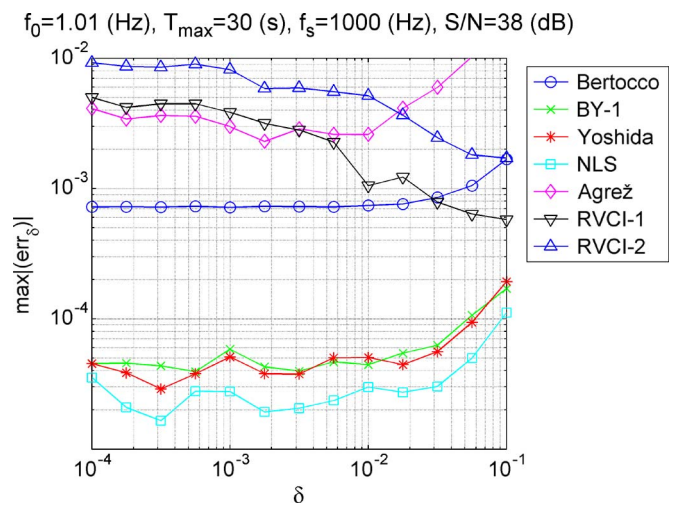


Fig. 4. Maximum error of the logarithmic decrement estimation.

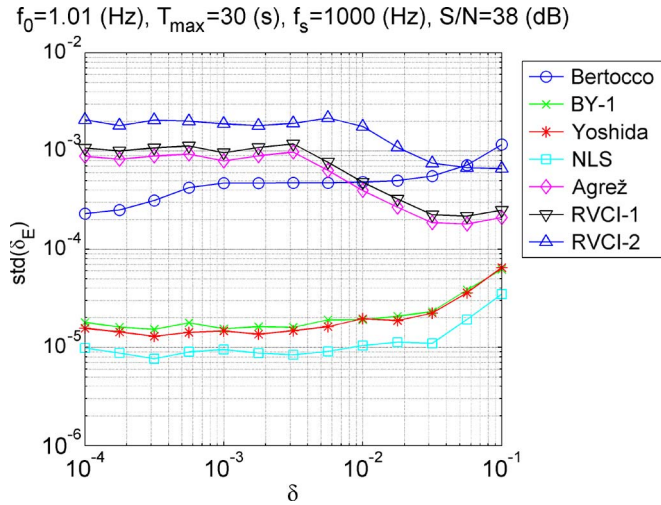


Fig. 5. STD of the logarithmic decrement estimation.

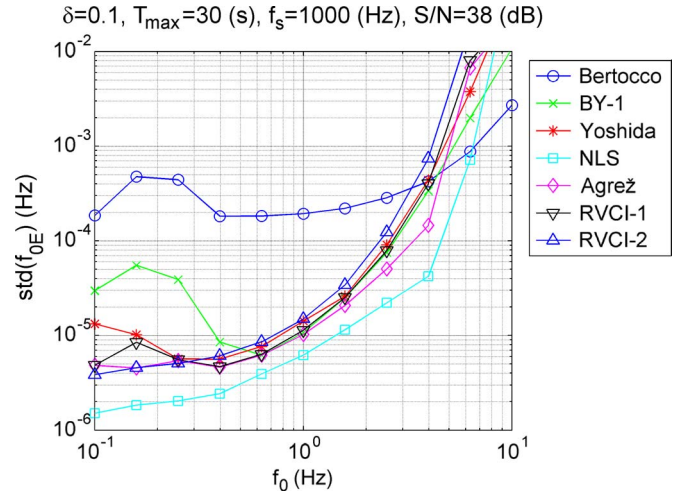


Fig. 7. STD of the resonant frequency estimation.

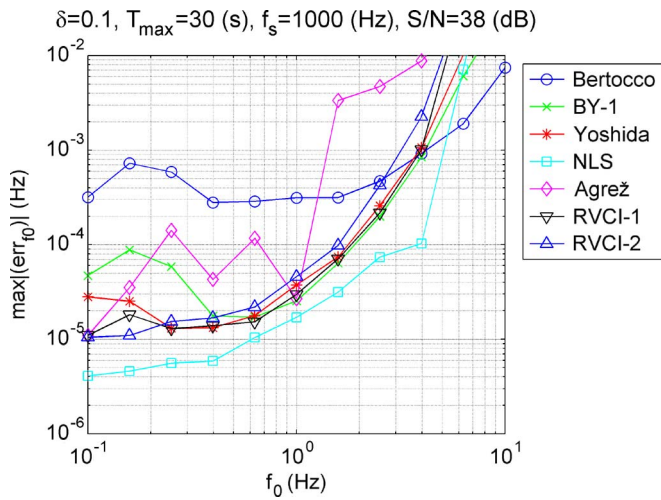


Fig. 6. Maximum error of the resonant frequency estimation.

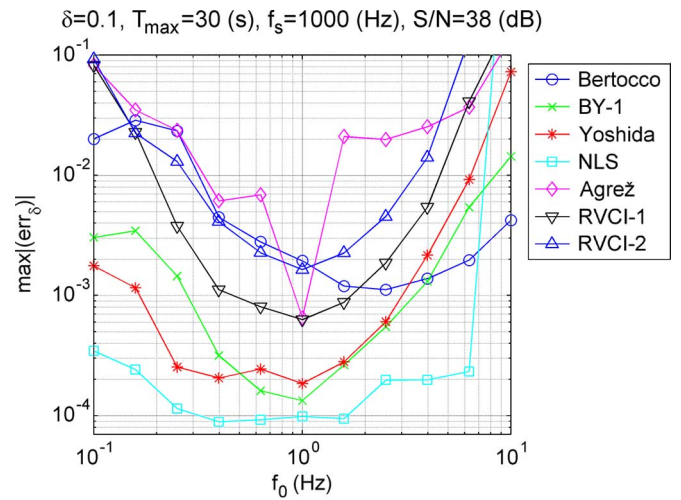


Fig. 8. Maximum error of the logarithmic decrement estimation.

The proposed RVCI-1 method performs similarly to the Yoshida method in f_0 estimation, and the proposed BY-1 method gives similar results to the Yoshida method in δ estimation.

For the special case of the coherent sampling $f_0 = 1$ Hz (not presented in figures), the best results in f_0 and δ estimation were obtained for the proposed BY-1 method, and the second place was taken by the Yoshida method.

B. Influence of the Resonant Frequency

In this section, we analyze the estimation errors for $\delta = 0.1$ as a function of f_0 . Figs. 6 and 7 and Figs. 8 and 9 show the maximum error and the STD of f_0 and δ estimation, respectively.

For $f_0 = 1$ Hz, test signals are coherently sampled. This is observed in Figs. 6–9 as a local minimum for the Agrež method; unfortunately for noncoherent sampling, this method is severely biased. By fixing acquisition time, we can see an increase in the estimation errors with the resonant frequency f_0 (see Figs. 6–9) due to increasing value of damping $\beta = \delta f_0 / f_s$. In turn, for

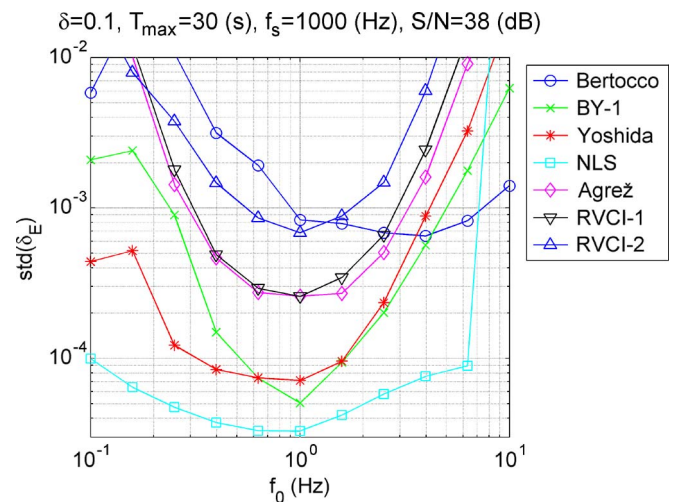


Fig. 9. STD of the logarithmic decrement estimation, for f_0 from 0.1 to 10 Hz.

very small values of f_0 , estimation quality of δ is getting worse due to decreasing number of oscillations present in the analyzed time interval.

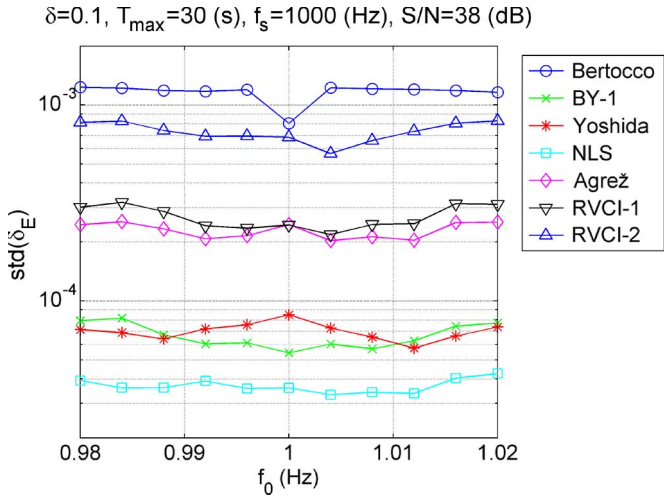


Fig. 10. STD of the logarithmic decrement estimation, for f_0 from 0.98 to 1.02 Hz.

The best results for the coherent sampling were obtained for the proposed BY-1 method.

Fig. 10 depicts the STD of the δ estimation for frequencies f_0 in the close neighborhood of coherent sampling, which occurs for $f_0 = 1$ Hz. For close-to-coherent sampling conditions, the proposed BY-1 method has the lowest STD of δ . A similar property was observed (but is not presented) for the f_0 estimation. In practice, such conditions are easy to obtain by appending a vector of zeros with appropriate length at the end of a signal before DFT computation.

C. Influence of the ZPD

In this section, we compute the errors induced by the ZPD [5], [6]. We aim at comparing robustness of the DFT-based methods against the ZPD. The ZPD is modeled by a linear function as follows:

$$\varepsilon_{ZPD}(t) = aAt/T_{max} \tag{21}$$

where $T_{max} = 30$ s, and a is a constant that determines “the strength” of the ZPD. Likewise, in simulations, other extrinsic functions may be also used, such as parabolic, power law, or exponential. Of course, it is not guaranteed that an *a priori* selected function corresponds to the physically meaningful ZPD (“self-microtwisting” of a sample [5]) embedded in the analyzed free decaying signal.

Figs. 11 and 12 show the maximum error and the STD of the δ estimation as a function of the ZPD “strength,” respectively. Results for f_0 (not shown) are similar. The best results are obtained for the Yoshida method, although for a weak ZPD, the proposed BY-1 method yields similar results. The time-domain NLS optimization gives poor results for the analyzed free decaying signal $T_{max} = 30$ s as, in general, only a constant offset is included in the signal model. Yet, the NLS-based OMI can be successfully used for a short-time segment of a signal disturbed by the ZPD [5].

Since the ZPD is generally not possible to be included in the signal model, the NLS method loses against the DFT-based

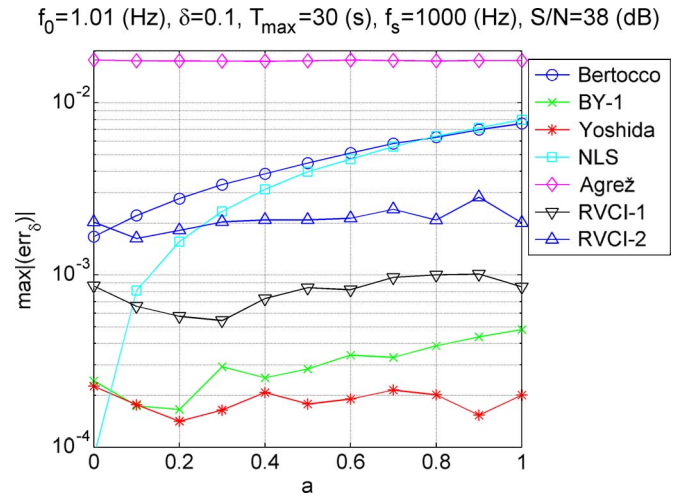


Fig. 11. Maximum error of the logarithmic decrement estimation.

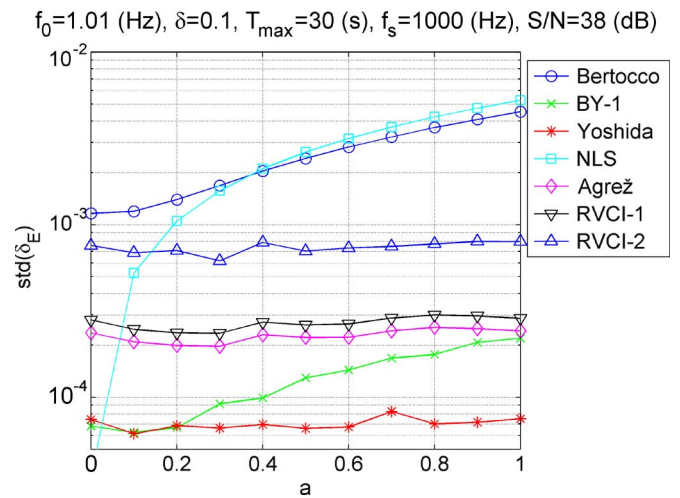


Fig. 12. STD of the logarithmic decrement estimation.

methods. For the DFT-based methods, the separation of the signal of interest from any disturbance is much easier as it is done in the frequency domain.

D. Systematic Errors

In this section, we show the systematic errors of the DFT-based methods described in this paper. Systematic errors are computed for ideal test signals, i.e., $\varepsilon_w[n] = 0$, $\varepsilon_{dc}[n] = 0$, and $\varepsilon_{ZPD}[n] = 0$, and for that reason, they are not of primary concern in mechanical spectroscopy, where we always analyze noise-free decaying oscillations.

However, systematic errors are important in other applications for signals with a higher S/N ratio. It is also interesting to observe bias–variance tradeoff of the estimators, e.g., the Yoshida algorithm is ordinary in the sense of systematic errors, but it is excellent in the sense of noise immunity for the previously analyzed case of $S/N = 38$ dB.

Systematic errors, when small as expected, are also good validation of derivation (i.e., assumed approximations) and implementation of the algorithms.

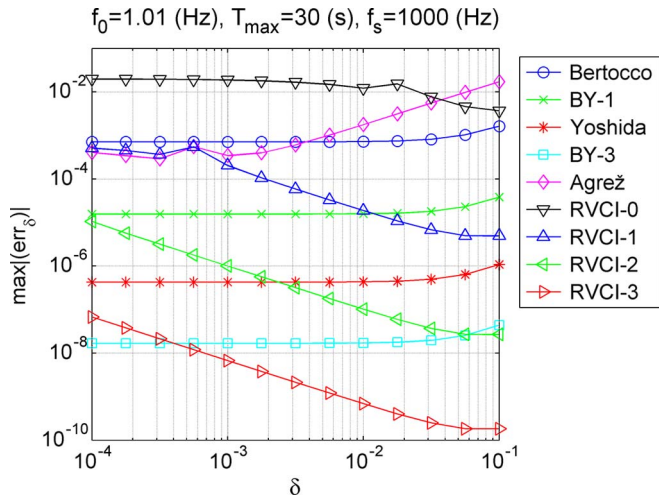


Fig. 13. Maximum systematic error of the logarithmic decrement estimation.

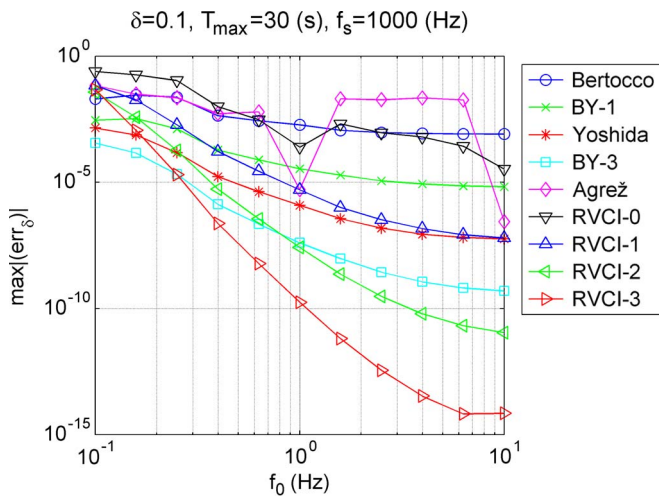


Fig. 14. Maximum systematic error of the logarithmic decrement estimation.

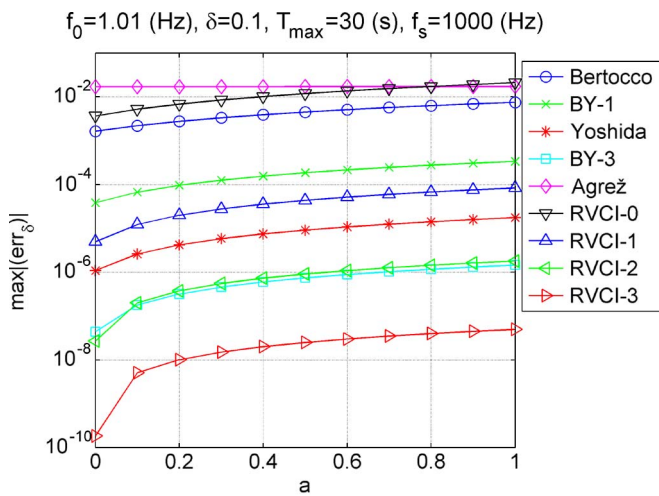


Fig. 15. Maximum systematic error of the logarithmic decrement estimation.

As before, 100 test signals with a uniformly distributed random phase were generated for different values of resonant frequency and logarithmic decrements. Maximum estimation systematic errors are shown in Figs. 13–15.

In all cases, increasing the order of a BY- M or an RVCi- M method results in significant reduction in systematic errors. It is also observed that the Agrež algorithm works well only when the signal is coherently sampled, i.e., $f_0 = 1$ Hz, for which case it is practically equivalent to the RVCi-1 method (see Fig. 14).

Figs. 13–15 clearly indicate that the proposed algorithms have significantly lower systematic errors than the other methods reported in the literature.

IV. CONCLUSION

In this paper, an important family of DFT-based algorithms for the parameter estimation of exponentially damped sinusoids has been reviewed, and two new nonparametric methods have been presented. The algorithms have been tested on time-domain data encountered in low-frequency resonant mechanical spectroscopy and shown good performance in the parameter estimation. For the proposed BY- M and RVCi- M methods, systematic errors may be arbitrarily small for sufficiently high-order M .

In the case of noisy measurements, the resonant frequency f_0 and the logarithmic decrement δ can be estimated with higher accuracy and lower STD by the proposed BY-1 than by the Yoshida method for the easy-to-be-obtained close-to-coherent conditions.

Obviously, for experimentally justified cases, an increase in the sampling frequency f_s (e.g., from 1 to 5 kHz) reduces the variance of f_0 and δ for all methods analyzed in this paper.

The results presented in this paper exhibit that the Agrež method offers good f_0 estimation performance only for coherent sampling, whereas the proposed RVCi-1 algorithm is superior among DFT-based f_0 estimation methods for noncoherent sampling. By contrast, the Yoshida method has confirmed its superiority (among the DFT-based approaches) in logarithmic decrement estimation. However, the proposed BY-1 method may have lower STD for close-to-coherent sampling.

It was also demonstrated that the Bertocco method is a poor estimator, as compared with other DFT-based methods.

The DFT-based estimation of resonant frequency and logarithmic decrements should be preferred over optimization-based NLS when processing time is a limiting factor. Indeed, in performed simulations, the DFT-based estimation was, on average, more than 140 times faster (for $N = 30\,000$ samples) than the NLS one initialized by the RVCi-1, and still, the variance of estimation was reasonably low compared with the optimal NLS.

DFT-based estimation should also be preferred over a time-domain NLS optimization when a measurement signal is expected to contain undesirable components [11] that cannot be included in a signal model. In this paper, we analyzed the ZPD, which is the crucial problem for shape memory alloys and *in situ* deformed metallic samples [5], [6], [10]. The difficulty of model selection is the major drawback of all parametric methods.

When computational time is not a concern, the DFT-based methods should be used to provide a good starting point to the NLS optimization and thus to improve significantly optimization convergence.

Although not discussed in the paper, the DFT-based methods can also be used to analyze multicomponent signals in various spectroscopic techniques. In such case, spectral leakage from neighboring frequencies may be effectively reduced by the proposed RVCI- M method.

The NLS optimization may also be conducted in the frequency domain. For a rectangular window, the cost function defined with all DFT bins is an optimal estimator of signal parameters and is equivalent to the optimization of (3) [25]. Unmodeled disturbances such as the general ZPD may be removed from the cost function by discarding proper DFT bins. Spectral leakage from unmodeled disturbances may be reduced by appropriate time windows. However, using a window other than the rectangular one and reducing the number of DFT bins in the cost function decreases statistical efficiency, and the estimator is no longer optimal; this is a well-known bias-variance tradeoff. The theoretical DFT spectrum of the damped sinusoidal signal analyzed with an arbitrary cosine window may be derived easily with the concept of the damped time window introduced in this paper.

APPENDIX A

The DFT of the signal (4) analyzed with the rectangular window is given by [25]

$$V[k] = \frac{A}{2} \left(e^{j\varphi} \frac{1 - \lambda^N}{1 - \lambda e^{-j\omega_k}} + e^{-j\varphi} \frac{1 - \lambda^{*N}}{1 - \lambda^* e^{-j\omega_k}} \right) \quad (A1)$$

where $\lambda = e^{-\beta + j\omega_0}$, $\omega_k = (2\pi/N)k$, and an asterisk stands for the complex conjugate value. We assume that spectral leakage from the negative frequencies can be neglected. Therefore, the DFT spectrum (A1) is approximated by

$$V[k] \approx \frac{A}{2} \left(e^{j\varphi} \frac{1 - \lambda^N}{1 - \lambda e^{-j\omega_k}} \right). \quad (A2)$$

Let us compute the following ratio of the first-order differences of the DFT bins:

$$R = \frac{V[k-1] - V[k]}{V[k] - V[k+1]} = \frac{1 - \lambda e^{-j\omega_{k+1}}}{1 - \lambda e^{-j\omega_{k-1}}} r$$

$$r = \frac{-e^{-j\omega_k} + e^{-j\omega_{k-1}}}{-e^{-j\omega_{k+1}} + e^{-j\omega_k}}. \quad (A3)$$

From (A3), we get the following:

$$\lambda = e^{j\omega_k} \frac{r - R}{r e^{-j2\pi/N} - R e^{j2\pi/N}}. \quad (A4)$$

Damping and frequency are next computed as

$$\beta = -\text{Re} \{ \ln(\lambda) \} \quad \text{and} \quad \omega_0 = \text{Im} \{ \ln(\lambda) \}. \quad (A5)$$

Going the same pattern with the ratio of the third-order differences, we get the following:

$$R = \frac{V[k-2] - 3V[k-1] + 3V[k] - V[k+1]}{V[k-1] - 3V[k] + 3V[k+1] - V[k+2]}$$

$$= \frac{1 - \lambda e^{-j\omega_{k+2}}}{1 - \lambda e^{-j\omega_{k-2}}} r \quad (A6)$$

where

$$r = r_1 / r_2$$

$$r_1 = (1 - \lambda e^{-j\omega_{k-1}})(1 - \lambda e^{-j\omega_k})(1 - \lambda e^{-j\omega_{k+1}})$$

$$- 3(1 - \lambda e^{-j\omega_{k-2}})(1 - \lambda e^{-j\omega_k})(1 - \lambda e^{-j\omega_{k+1}})$$

$$+ 3(1 - \lambda e^{-j\omega_{k-2}})(1 - \lambda e^{-j\omega_{k-1}})(1 - \lambda e^{-j\omega_{k+1}})$$

$$- (1 - \lambda e^{-j\omega_{k-2}})(1 - \lambda e^{-j\omega_{k-1}})(1 - \lambda e^{-j\omega_k})$$

$$r_2 = (1 - \lambda e^{-j\omega_k})(1 - \lambda e^{-j\omega_{k+1}})(1 - \lambda e^{-j\omega_{k+2}})$$

$$- 3(1 - \lambda e^{-j\omega_{k-1}})(1 - \lambda e^{-j\omega_{k+1}})(1 - \lambda e^{-j\omega_{k+2}})$$

$$+ 3(1 - \lambda e^{-j\omega_{k-1}})(1 - \lambda e^{-j\omega_k})(1 - \lambda e^{-j\omega_{k+2}})$$

$$- (1 - \lambda e^{-j\omega_{k-1}})(1 - \lambda e^{-j\omega_k})(1 - \lambda e^{-j\omega_{k+1}}) \quad (A7)$$

and λ is approximated by (A4). From (A6), we get the following:

$$\lambda = e^{j\omega_k} \frac{r - R}{r e^{-j2(2\pi/N)} - R e^{j2(2\pi/N)}}. \quad (A8)$$

Damping and frequency are computed from (A5) as before.

APPENDIX B

Let us define the damped time window $\bar{w}[n] = w[n]Ae^{-\beta n}$; then, (4) may be rewritten as

$$v[n] = \bar{W}[n]A \cos(\omega_0 n + \varphi). \quad (B1)$$

The continuous theoretical spectrum of the windowed discrete time signal (B1) is given by [22]

$$V(e^{j\omega}) = \frac{A}{2} e^{j\varphi} \bar{W} \left(e^{j(\omega - \omega_0)} \right) + \frac{A}{2} e^{-j\varphi} \bar{W} \left(e^{j(\omega + \omega_0)} \right) \quad (B2)$$

where $\bar{W}(e^{j\omega})$ is the spectrum of the damped window $\bar{w}[n]$, and $0 \leq \omega < \pi$.

The spectrum of the rectangular window is given by [22]

$$W_0(e^{j\omega}) = \sum_{n=0}^{N-1} e^{-j\omega n} = e^{-j\omega(N-1)/2} \frac{\sin(\omega N/2)}{\sin(\omega/2)}. \quad (B3)$$

Using (B3), the spectrum of the damped rectangular window is as follows:

$$\bar{W}_0(e^{j\bar{\omega}}) = \sum_{n=0}^{N-1} e^{-\beta n} e^{-j\omega n} = e^{-j\bar{\omega}(N-1)/2} \frac{\sin(\bar{\omega} N/2)}{\sin(\bar{\omega}/2)} \quad (B4)$$

where $\bar{\omega} = \omega - j\beta$. For damping $\beta = 0$, we get the spectrum of the rectangular window in (B4).

Theoretical spectrum of the arbitrary cosine window (16) may be computed as a sum of the frequency shifted and the rescaled spectra of the rectangular window. As an example, let us consider the Hann window. This window may be interpreted as a sum of the rectangular window with the

rectangular window shifted to frequency $2\pi/N$, namely as follows:

$$w_1[n] = 1 - \cos((2\pi/N)n) = w_0[n] - w_0[n] \cos((2\pi/N)n). \quad (\text{B5})$$

The spectrum of the Hann window from (B5) and (B2) is as follows:

$$W_1(e^{j\omega}) = -\frac{1}{2}W_0(e^{j(\omega-\omega_1)}) + W_0(e^{j\omega}) - \frac{1}{2}W_0(e^{j(\omega+\omega_1)}) \quad (\text{B6})$$

with $\omega_1 = 2\pi/N$. Generally, the spectrum of the arbitrary periodic cosine window (16) is as follows:

$$W_M(e^{j\omega}) = \sum_{m=0}^M (-1)^m \frac{A_w[m]}{2} W_0(e^{j(\omega-\omega_m)}) + (-1)^m \frac{A_w[m]}{2} W_0(e^{j(\omega+\omega_m)}) \quad (\text{B7})$$

with $\omega_m = (2\pi/N)m$, and the spectrum of the damped cosine window is as follows:

$$\overline{W}_M(e^{j\bar{\omega}}) = \sum_{m=0}^M (-1)^m \frac{A_w[m]}{2} \overline{W}_0(e^{j(\bar{\omega}-\omega_m)}) + (-1)^m \frac{A_w[m]}{2} \overline{W}_0(e^{j(\bar{\omega}+\omega_m)}). \quad (\text{B8})$$

We assume that spectral leakage from negative frequencies can be neglected. Therefore, the continuous theoretical spectrum of the windowed discrete time signal (B1) is approximated by

$$V(e^{j\omega}) \approx \frac{A}{2} e^{j\varphi} \overline{W}(e^{j(\omega-\omega_0)}). \quad (\text{B9})$$

Using (B9), the ratios defined by (19) are as follows:

$$R_1 = \frac{|V[k+1]|^2}{|V[k]|^2} \approx \frac{|\overline{W}(\omega_{k+1})|^2}{|\overline{W}(\omega_k)|^2} \\ R_2 = \frac{|V[k-1]|^2}{|V[k]|^2} \approx \frac{|\overline{W}(\omega_{k-1})|^2}{|\overline{W}(\omega_k)|^2} \quad (\text{B10})$$

where $V[k]$ has the highest magnitude, and $V[k+1]$ and $V[k-1]$ are the second and the third DFT bins with the highest magnitude, respectively. Using the ratios R_1 and R_2 , we freed the problem from the amplitude and phase parameters.

Using the frequency correction d defined by (6), we have the following:

$$\omega_{k-1} = \omega_0 - d2\pi/N - 2\pi/N \\ \omega_k = \omega_0 - d2\pi/N \\ \omega_{k+1} = \omega_0 - d2\pi/N + 2\pi/N \quad (\text{B11})$$

where ω_0 is the signal frequency. The desired formulas for (17) and (18) are obtained by putting (B11) into (B10) and solving for d and β . The derivation for the higher order RVCI windows require space-consuming algebra, and for this reason, we only

show the solution for RVCI order 0 and RVCI order 1; for higher orders, the derivation goes in the same pattern.

For the damped rectangular window (RVCI, $M = 0$) in (B4) and (B11), we have the following:

$$|\overline{W}_0(\omega_{k-1})| \approx e^{-\beta(N-1)/2} \frac{N}{\pi} \frac{|\sin(-d\pi + \beta N/(2j))|}{|-d-1-jB|} \\ |\overline{W}_0(\omega_k)| \approx e^{-\beta(N-1)/2} \frac{N}{\pi} \frac{|\sin(-d\pi + \beta N/(2j))|}{|-d-jB|} \\ |\overline{W}_0(\omega_{k+1})| \approx e^{-\beta(N-1)/2} \frac{N}{\pi} \frac{|\sin(-d\pi + \beta N/(2j))|}{|-d+1-jB|} \quad (\text{B12})$$

where $B = \beta N/(2\pi)$, and we assumed that the arguments of the sinusoidal functions are small enough to be replaced by their arguments. Using (B12), the ratios (B10) are as follows:

$$R_1 = \frac{d^2 + B^2}{(d-1)^2 + B^2} \quad \text{and} \quad R_2 = \frac{d^2 + B^2}{(d+1)^2 + B^2}. \quad (\text{B13})$$

Solving (B13) for d and β , we get (17) and (18) for $M = 0$.

For the damped Hann window (RVCI, $M = 1$) in (B6), we have the following:

$$|\overline{W}_1(e^{j\omega})| = e^{-\beta(N-1)/2} \left| \sin\left(\frac{\omega N}{2} + \beta \frac{N}{2j}\right) \right| \\ \times \left| -\frac{0.5}{\sin\left(\frac{\omega}{2} + \frac{\beta}{2j} - \frac{\pi}{N}\right)} + \frac{1}{\sin\left(\frac{\omega}{2} + \frac{\beta}{2j}\right)} - \frac{0.5}{\sin\left(\frac{\omega}{2} + \frac{\beta}{2j} + \frac{\pi}{N}\right)} \right|. \quad (\text{B14})$$

Putting (B11) into (B14) and computing (B10) give the following:

$$R_1 = \frac{(d+1)^2 + B^2}{(d-2)^2 + B^2} \quad \text{and} \quad R_2 = \frac{(d-1)^2 + B^2}{(d+2)^2 + B^2}. \quad (\text{B15})$$

By solving (B15) for d and β , we get (17) and (18) for $M = 1$.

REFERENCES

- [1] A. S. Nowick and B. S. Berry, *Anelastic Relaxation in Crystalline Solids*. New York: Academic, 1972.
- [2] L. B. Magalas, "Mechanical spectroscopy—Fundamentals," *Solid State Phenom.*, vol. 89, pp. 1–22, 2003.
- [3] L. B. Magalas, "Mechanical spectroscopy, internal friction and ultrasonic attenuation: Collection of works," *Mater. Sci. Eng. A*, vol. 521/522, pp. 405–415, Sep. 2009.
- [4] S. Etienne, S. Elkoun, L. David, and L. B. Magalas, "Mechanical spectroscopy and other relaxation spectroscopies," *Solid State Phenom.*, vol. 89, pp. 31–66, 2003.
- [5] L. B. Magalas and M. Majewski, "Ghost internal friction peaks, ghost asymmetrical peak broadening and narrowing: Misunderstandings, consequences and solution," *Mater. Sci. Eng. A*, vol. 521–522, pp. 384–388, Sep. 2009.
- [6] L. B. Magalas and A. Pilat, "Zero-point drift in low-frequency mechanical spectroscopy," *Solid State Phenom.*, vol. 115, pp. 285–292, 2006.

- [7] L. B. Magalas and T. Malinowski, "Measurement techniques of the logarithmic decrement," *Solid State Phenom.*, vol. 89, pp. 247–260, 2003.
- [8] L. B. Magalas, "Determination of the logarithmic decrement in mechanical spectroscopy," *Solid State Phenom.*, vol. 115, pp. 7–14, 2006.
- [9] L. B. Magalas and M. Majewski, "Recent advances in determination of the logarithmic decrement and the resonant frequency in low-frequency mechanical spectroscopy," *Solid State Phenom.*, vol. 137, pp. 15–20, 2008.
- [10] L. B. Magalas, "The Snoek–Köster relaxation. New insights—New paradigms," *J. Phys. IV*, vol. 6, no. C8, pp. C8-163–C8-172, Dec. 1996.
- [11] I. Yoshida, T. Sugai, S. Tani, M. Motegi, K. Minamida, and H. Hayakawa, "Automation of internal friction measurement apparatus of inverted torsion pendulum type," *J. Phys. E, Sci. Instrum.*, vol. 14, no. 10, pp. 1201–1206, Oct. 1981.
- [12] M. Bertocco, C. Offelli, and D. Petri, "Analysis of damped sinusoidal signals via a frequency-domain interpolation algorithm," *IEEE Trans. Instrum. Meas.*, vol. 43, no. 2, pp. 245–250, Apr. 1994.
- [13] D. Agrež, "A frequency domain procedure for estimation of the exponentially damped sinusoids," in *Proc. Int. Instrum. Meas. Technol. Conf.*, May 2009, pp. 1321–1326.
- [14] E. Aboutanios, "Estimation of the frequency and decay factor of a decaying exponential in noise," *IEEE Trans. Signal Process.*, vol. 58, no. 2, pp. 501–509, Feb. 2010.
- [15] V. H. Jain, W. L. Collins, and D. C. Davis, "High accuracy analog measurement via interpolated FFT," *IEEE Trans. Instrum. Meas.*, vol. IM-28, no. 2, pp. 113–122, Jun. 1979.
- [16] T. Grandke, "Interpolation algorithms for discrete Fourier transform of weighted signals," *IEEE Trans. Instrum. Meas.*, vol. IM-32, no. 2, pp. 350–355, Jun. 1983.
- [17] G. Andria, M. Savino, and A. Trotta, "Windows and interpolation algorithms to improve electrical measurement accuracy," *IEEE Trans. Instrum. Meas.*, vol. 38, no. 4, pp. 856–863, Aug. 1989.
- [18] C. Offelli and D. Petri, "Interpolation techniques for real-time multifrequency waveform analysis," *IEEE Trans. Instrum. Meas.*, vol. 39, no. 1, pp. 106–111, Feb. 1990.
- [19] D. Agrež, "Weighted multipoint interpolated DFT to improve amplitude estimation of multifrequency signal," *IEEE Trans. Instrum. Meas.*, vol. 51, no. 2, pp. 287–292, Apr. 2002.
- [20] D. Belega and D. Dallet, "Amplitude estimation by a multipoint interpolated DFT approach," *IEEE Trans. Instrum. Meas.*, vol. 58, no. 5, pp. 1316–1323, May 2009.
- [21] K. Duda, "DFT interpolation algorithm for Kaiser–Bessel and Dolph–Chebyshev windows," *IEEE Trans. Instrum. Meas.*, vol. 60, no. 3, pp. 784–790, Mar. 2011.
- [22] A. V. Oppenheim, R. W. Schaffer, and J. R. Buck, *Discrete-Time Signal Processing*, 2nd ed. Englewood Cliffs, NJ: Prentice-Hall, 1999.
- [23] F. J. Harris, "On the use of windows for harmonic analysis with the discrete Fourier transform," *Proc. IEEE*, vol. 66, no. 1, pp. 51–83, Jan. 1978.
- [24] Y. Yao and S. M. Pandit, "Cramér–Rao lower bounds for a damped sinusoidal process," *IEEE Trans. Signal Process.*, vol. 43, no. 4, pp. 878–885, Apr. 1995.
- [25] R. Pintelon and J. Schoukens, *System Identification: A Frequency Domain Approach*. Piscataway, NJ: IEEE Press, 2001.



Krzysztof Duda received the M.S. degree in automatics and metrology and the Ph.D. degree in electronics from Akademia Górniczo-Hutnicza University of Science and Technology (AGH-UST), Kraków, Poland, in 1998 and 2002, respectively.

Since 2002, he has been an Assistant Professor with the Department of Measurement and Instrumentation, AGH-UST. His research interests include applications of digital signal processing and analysis.

Leszek B. Magalas is a Professor of materials science with the Faculty of Metals Engineering and Industrial Computer Science, Akademia Górniczo-Hutnicza University of Science and Technology (AGH-UST), Kraków, Poland. His research interests include mechanical spectroscopy, materials science, and physical metallurgy.



Mariusz Majewski received the M.S. degree in applied computer science from Akademia Górniczo-Hutnicza University of Science and Technology (AGH-UST), Kraków, Poland, in 2006, where he is currently working toward the Ph.D. degree in materials engineering with the Faculty of Metals Engineering and Industrial Computer Science, AGH-UST.

His current research interests include digital signal analysis in mechanical spectroscopy.



Tomasz P. Zieliński (M'07) received the M.S. degree in electronics and the D.Sc. degree (habilitation) in electrical engineering from the Akademia Górniczo-Hutnicza University of Science and Technology (AGH-UST), Kraków, Poland, in 1982 and 1996, respectively, and the Ph.D. degree in electrical engineering from the Bulgarian Academy of Sciences, Sofia, Bulgaria, in 1988.

In 1982, he was with the Department of Measurement and Instrumentation and then with the Department of Telecommunications, AGH-UST, as a Research & Teaching Assistant. In 1989, he became an Associate Professor; in 1996, an Assistant Professor; in 2000, an Associate Professor; in 2003, a Professor in telecommunications; and in 2006, a Full Professor. He is the author or coauthor of more than 150 scientific journal and conference papers. He is also the author of three monographs (all in Polish): *Time–Frequency and Time–Scale Representations of Non-stationary Signals* (1996), *From Theory to Digital Signal Processing* (2002, 2004) and *Digital Signal Processing: From Theory to Applications* (2005, 2007, 2009). His research interests include advanced digital signal processing in telecommunication and biomedical systems, particularly time–frequency signal analysis.